Journal of Low Temperature Physics, Vol. 137, Nos. 5/6, December 2004 (© 2004)

Heat Inputs to Sub-mK Temperature Cryostats and Experiments from γ-Radiation and Cosmic Ray Muons

E. Nazaretski, V. O. Kostroun, S. Dimov, R. O. Pohl, and J. M. Parpia

Laboratory of Atomic and Solid State Physics, Cornell University, Ithaca, NY 14853 U.S.A.
E-mail: jmp9@cornell.edu

(Received May 5, 2004; revised September 16, 2004)

We measured the spectrum of energies deposited by γ-radiation, emanating from radioactive materials in the laboratory that houses our mK cryostat, and by cosmic ray muons. This allows us to quantify the heat input that adversely affects the lowest temperature accessible in sub-mK experiments. We use our nuclear stage, stage plate and experimental cell as a prototype "model" system, and calculate the power deposited due to low energy (below 2.65 MeV) background radiation γ quanta ($\sim$20 pW). This is significantly less than the power ($\sim$120 pW) deposited in the nuclear and experimental stages by muons. Installation of a 5 cm thick lead wall around the cryostat reduced the energy due to the flux of γ quanta by a factor of $\sim$10 to $\sim$2 pW, and the number of γ quanta by a factor of $\sim$20. The lower energy, "soft" cosmic ray component was also affected by introducing the same thickness of lead, reducing the overall count of cosmic ray derived particles by $\sim$15% and the heat leak to $\sim$100 pW.

KEY WORDS: ultra-low temperature, heat leaks, cosmic ray μ, γ.

1. INTRODUCTION

Over the past decades, the performance of nuclear demagnetization cryostats has improved significantly,[1,2] allowing access to temperatures well below 100 μK for an extended period of time. In a typical nuclear demagnetization cryostat, the ultimate temperature that can be achieved is set by the residual heat load and the thermal resistance of the nuclear stage. The thermal resistance arises from a combination of the bottleneck[3,4] between the conduction electrons and the nuclear spins (whose entropy is reduced by precooling in a magnetic field and where the cooling power resides) together with the electronic thermal resistivity of the

0022-2291/04/1200-0609/0

metallic portions of the cryostat. Regardless of which term dominates the thermal resistance, the lowest temperature that can be attained is critically dependent on the size of the heat load. In the best cryostats[1] the limiting heat load decreased to ~100 pW after several months of operation. The magnitude of this heat input is established by vibrations of the flexible parts of the cryostat in the magnetic field of the demgnetization magnet, by the time dependent "virtual heat leak" contributions due to long-time relaxation processes in glassy insulators,[5] and by the passage of μ cosmic rays that interact with the nuclear stage causing ionization and consequent heating of the cryostat. The design of a cryostat can be optimized to reduce the vibrational heat load and minimize the presence of glassy parts, but it is impossible to eliminate the contribution due to the charged particles originating from cosmic rays. We point out that there is another source of heating, namely that due to penetrating γ-radiation that is ubiquitous in laboratories, which has been ignored in the past. Here, we quantify this contribution as well as demonstrate that it is possible to shield out this potential source of heating by enclosing the cryostat in a 5 cm thick lead wall, which also reduces the "soft" component of cosmic rays.

The paper is organized as follows. We first describe our motivating experiment in which we found that the γ-radiation emanating from building materials had a significant effect. We measure the spectrum of γ-radiation in our laboratory with a conventional Ge detector, and outline how the energy deposited by the passage of γ (and in a later Section, by cosmic ray muons) may be calculated using our nuclear refrigerator as a model system. We follow with an overview of the background radiation due to cosmic ray muons, and briefly discuss the thermal gradients that would result from the deposited power.

2. OBSERVATION OF HEATING EFFECTS

Our original intent in carrying out these experiments was to examine the acoustic properties of amorphous silica over a temperature range between 1 and 100 mK. We used a composite torsional oscillator to study the acoustic properties of amorphous silica (Suprasil-W, <5 ppm molar OH^- impurities). The design of the experiment is similar to that of Cahill and van Cleve.[6] The lower part of the composite oscillator was made from quartz and was used to drive the upper amorphous silica part. The bottom end of the quartz driver was epoxied to a beryllium-copper base to allow freedom for torsional excursions, and functioned as an approximation of a free-end boundary condition. The length of the silica was tuned so that the joint between the silica and quartz is a nodal point. The AC drive frequency was swept through the resonance (~84 kHz) and the

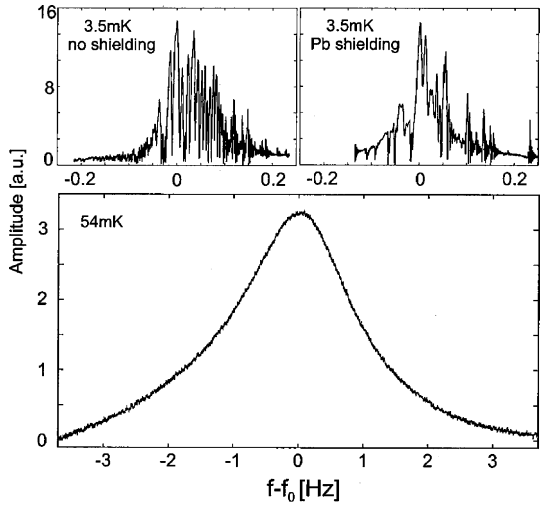

Fig. 1. Resonance spectra of the composite oscillator at different temperatures. At the lower temperature the resonance is affected by transients while at 54 mK it is free from "noise". The reduction in heat capacity accounts for the visibility of transients at low temperatures.[9] At top left we show the spectrum obtained at 3.5 mK without any lead shielding. The frequency of transients seen with the 5 cm thick lead shielding in place at top right is reduced by a factor of three compared to the unshielded response. Here f_0 denotes the resonance frequency ($\approx$85 kHz).

response was recorded using a lock-in amplifier, while the temperature was held constant. The oscillator was mounted on a nuclear demagnetization cryostat to access the mK regime. A ^{3}He melting curve thermometer was used to monitor the temperature of the cryostat and the sample. A more detailed description of the experiment can be found elsewhere.[7,8] Below 20 mK the behavior of the oscillator was strongly affected by the presence of the ambient radioactive background in the laboratory.[8,9] Figure 1 shows two sweeps through resonance taken at 3.5 mK without and with lead shielding while a sweep taken at 54 mK showed no effects of the background radiation.

The transients visible at low temperatures are due to interactions with cosmic rays and background radiation present in the laboratory. In refs. 8 and 9, we identified the background radiation as the major source of these transients following the observation that their frequency decreased by a factor of $\sim$3 (see Fig. 1) after we erected a shielding layer of 5 cm thick lead bricks around the cryostat. The remaining transients were attributed to the charged particle component of cosmic rays, primarily μ. The first instance where the effects of cosmic rays were observed in

ultra-low temperature apparatus is that discussed by Niinikoski,[10] and their influence has been shown to mediate the nucleation of the ^{3}He superfluid B phase,[11,12] and also vortices in ^{4}He.[13] We verified the effect of γ-radiation from the low-level background by exposing the cryostat to 6.1 μCi ^{22}Na and 6.5 μCi ^{137}Cs γ sources. This procedure increased the number of transients superposed on the resonance curve dramatically. We note that similar effects have been seen by us in a functionally identical composite oscillator, where the material under study was Stycast 1266.[14]

Another effect of γ-radiation on the oscillator was heating, inferred from the positive resonant frequency shift consistent with an overall increase of the sample temperature.[9,15] Thus γ-radiation (along with cosmic rays) cannot be ignored as a potential source of heating at ultra-low temperatures.

3. ENERGY FLUX FROM BACKGROUND γ-RADIATION

We measured the background γ-radiation level in our laboratory in the energy range 0.05 to 2.65 MeV with a liquid nitrogen cooled, 5.33 cm diameter × 6.6 cm long Ge detector that registers the energy deposited by energetic particles that strike it. The raw data was corrected for an energy dependent absorption factor, p (described below) and we show two spectra in Fig. 2, one taken without any shielding (upper set) and the second (lower set) taken with a 5 cm thick lead wall around the cryostat. The nearly horizontal "lines" visible in the figure are due to the discrete nature of the counting and the small energy width of each channel. Thus, some channels register only a single count even after 7200 seconds.

The photon scattering cross section[16] in Ge is reduced for more energetic γ rays and is listed in tables (for example, see Ref. 17) as $\sigma_{\mathrm{tot},t}$ with units of barns atom^{-1}(1×10^{-24} cm^2 atom^{-1}) and in the somewhat non-intuitive (but more useful) $(\mu/\rho)_{\mathrm{tot},t}$ (units of cm^2 g^{-1}). To convert units, the cross section in barns atom^{-1} is multiplied by the number of atoms gram^{-1}. For example for 1 MeV γ interacting with the Ge,

$$\begin{aligned}(\mu/\rho)_{\mathrm{tot},t} &= \sigma_{\mathrm{tot},t} \times N_{\mathrm{A}}/A \\ &= (6.90 \times 10^{-24}\ \mathrm{cm}^2\ \mathrm{atom}^{-1}) \\ &\quad \times (6.023 \times 10^{23}\ \mathrm{atoms\ mol}^{-1})/(72.59\ \mathrm{g\ mol}^{-1}) \\ &= 0.0572\ \mathrm{cm}^2\ \mathrm{g}^{-1}, \end{aligned} \tag{1}$$

where N_{A} is Avogadro's number, and A denotes the atomic weight in g. The cross section $(\mu/\rho)_{\mathrm{tot},t}$ contains contributions from the bound electron total incoherent (Compton) scattering (dominant near 1 MeV), pair production (dominant above 10 MeV) and the photoelectric and coherent

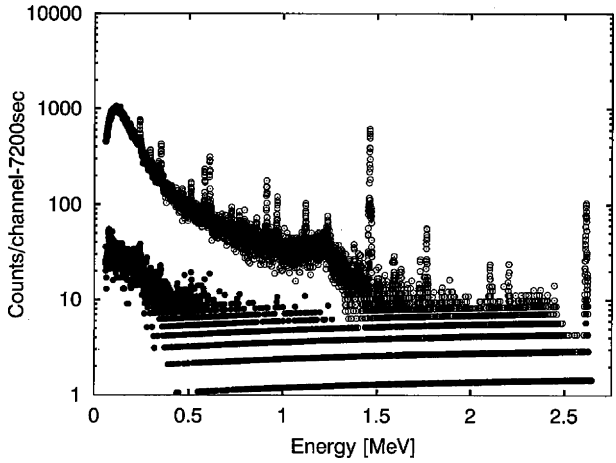

Fig. 2. Spectra of the background radiation in the laboratory. The upper spectrum represents the unshielded case. The lower spectrum was taken inside a 5 cm thick lead wall. Peaks associated with radioactivity in building materials (^{40}K—1.46 MeV, ^{228}Ac—0.908 and 0.967 MeV (the latter is the daughter nucleus of ^{232}Th)) are visible, as is a peak at 1.76 MeV associated with ^{214}Bi, daughter nucleus of ^{226}Ra. The highest energy γ emitted as the result of a naturally occurring decay process is the 2.615 MeV γ from the decay of ^{208}Tl in the thorium series. Other peaks in the spectrum can, in principle, be linked to specific elemental decays, but were not very prominent. Each "bin" corresponds to a channel (of energy width ~0.39 keV) in the multi-channel analyzer. The nearly horizontal "lines" (prominent in the shielded spectrum) correspond to the discrete nature of the counts and reflect the correction factor to the sensitivity of the Ge detector described in the text.

(Rayleigh) scattering (dominant below 0.5 MeV). The cross section establishes the absorption factor, p, for a γ passing through a length l of the germanium (density ρ_{Ge}),

$$p = 1 - \exp(-(\mu/\rho)_{\mathrm{tot},t}\rho_{\mathrm{Ge}}l). \tag{2}$$

For a large detector (or low energy) the probability of absorption is nearly unity. It we take the track length to be the diameter of the crystal (5.33 cm), p, for 1 MeV γ is 0.803. To compensate for the reduced absorption probability, an energy dependent correction p^{-1}, has to introduced, and approached 45% for the most energetic γ rays in this detector. The γ flux (0.61 γ cm^{-2} after these corrections) measured with the Ge detector (see Fig. 2), is comparable to the ~0.33 γ cm^{-2}s recorded with a 25.4 cm diameter × 25 cm long NaI detector at Heidelberg over the same energies.[18] The discrepancy is likely due to variations in the background from the different building materials used in these laboratories, and cannot be attributed to errors.

An examination of Fig. 2 reveals many sharp peaks in the unshielded spectrum. We resolved peaks associated with radioactivity in building materials (^{40}K decay emits 1.46 MeV γ-radiation, ^{228}Ac (daughter nucleus of ^{232}Th) yields 0.909 and 0.967 MeV γ, as well as a peak associated with ^{214}Bi, daughter nucleus of ^{226}Ra (yielding 1.76 MeV) γ-radiation.[19] Very similar peaks were seen in other investigations.[18,20–21] We note that the highest energy γ emitted as the result of a naturally occurring decay process is the 2.615 MeV γ emitted from the decay of ^{208}Tl in the thorium series. This energy thus serves as the natural boundary between decays due to radioactivity and the energy deposited by cosmic ray muons, discussed in Sec. 4.

Enclosing the cryostat and Ge detector in a 5 cm thick lead structure reduced the total count rate by a factor of $\sim$20 (see Fig. 2), consistent with p (see Eq. (2)) for lead, which has a high photon absorption cross section, and thus preferentially absorbs most low energy γ and also many of the higher energy γ quanta. The reduction in total count rate seen with the Ge detector is much larger than the observed factor of three reduction of the transient number in Fig. 1. The discrepancy originates in the contribution due to the μ charged particle component of cosmic rays whose spectrum will be discussed in Sec. 4.

Spectra shown in Fig. 2 can be used to estimate the heat load due to γ-radiation on our model copper nuclear demagnetization stage together with the experimental stage plate and large experimental cell. The dimensions of our nuclear stage (Fig. 3) $r=2$ cm, $l=45$ cm, and a fill factor of $\sim$0.9 give a mass 4.5 kg. We also assume an experimental chamber (with only a small cavity for ^{3}He) fabricated from silver with a 5 cm diameter, and 12.5 cm in length mounted on a 1.25 cm thick, 12.5 cm diameter stage plate.

Several factors have to be taken into account before the heat load can be estimated. The first is the absorption of the γ-radiation as it passes through the various materials of which the cryostat is constructed. We calculated the fraction transmitted (or transmission factor) s, from

$$s=\exp(-(\mu/\rho)_{tot,t,x}\,\rho_x\,l_x). \tag{3}$$

Here $(\mu/\rho)_{\mathrm{tot},t,x}$ is the photon scattering cross section and the additional subscript, x, denotes the element that the photons are interacting with, so that ρ_x is the density of the material, and l_x is the length of intervening material. We have to consider the transmission factor of the high field demagnetization magnet (which surrounds the nuclear stage) as well as that of the other construction materials (0.15 cm of copper in the vacuum can, 0.3 cm of aluminum in the dewar walls) together with

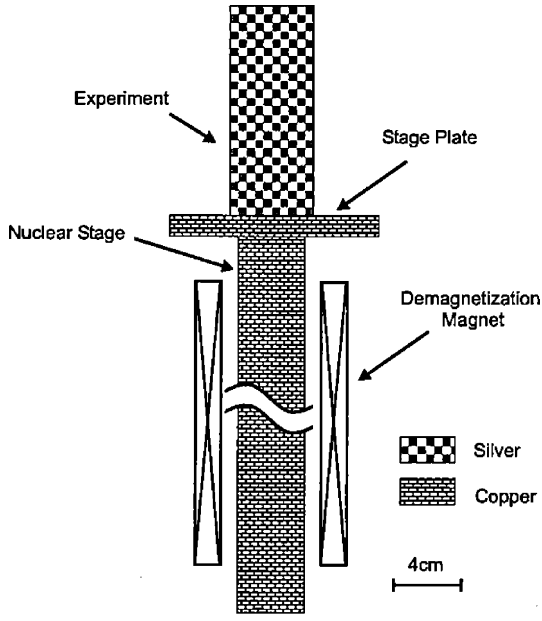

Fig. 3. Schematic diagram of a typical nuclear stage including the copper stage plate to which experiments are mounted.

0.02 cm each of niobium and titanium and 0.05 cm of copper in the compensation windings of the magnet as well as a further 2 mm thickness of aluminum in the former of the magnet. If we make the assumption that the high-field region of the magnet consists of a 3.1 cm radial thickness of winding of 80% copper-clad 20% Nb–Ti wire on a 0.6 cm thick aluminum former, we find the energy dependent transmission factor shown in Fig. 4, where the individual transmission factors for the various contributions, together with the overall value of s, are shown. Happily (for low temperature physicists), Fig. 4 shows that the copper in the magnet strongly attenuates the number of γ that would otherwise deposit energy into the nuclear stage.

Once s is calculated, we can estimate the energy deposited due to radiation present in the laboratory. The tables[17] provide information on the energy absorption cross section $(\mu/\rho)_{\mathrm{tot,en},x}$ for the element (x) with which the photons interact. We note that the photon scattering cross sections and energy absorption cross sections are not identical, since the energy of a scattered γ is not necessarily absorbed in the material. The latter cross section is useful in absorbed dose and radiation-effect determinations, and is obtained by summing the contributions of the bound

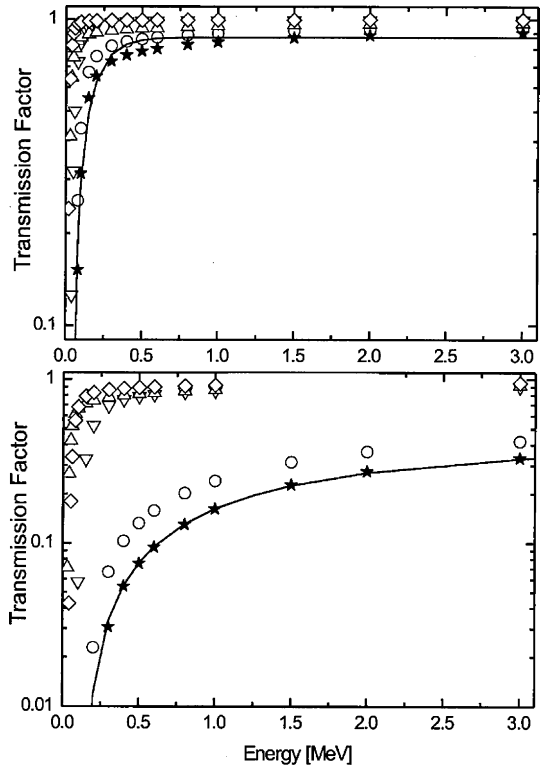

Fig. 4. The calculated transmission factor (fraction of γ quanta transmitted) as a function of the energy of γ-radiation as it passes through the various cryostat components excluding (top panel) and including (bottom panel) the demagnetization magnet. In both cases ($\diamond$) correspond to titanium, ($\triangle$) to aluminum, ($\triangledown$) to niobium, ($\circ$) to copper and ($\star$) to the overall transmission factor approximated by the fit (solid line). The metal in the magnet significantly reduces the γ-radiation that impacts the nuclear stage.

electron incoherent absorption, the pair production absorption, and the photoelectric absorption coefficients. The energy absorption factor is given below

$$E_{abs}/E_{\gamma} = 1 - \exp(-(\mu/\rho)_{\mathrm{tot,en,x}}\, \rho_x\, l_x). \tag{4}$$

The energy deposited is obtained by multiplying the incident γ spectrum energy by the transmission factor and the energy absorption factor (Eq. (4)). In the event that there is no external lead shielding mounted around the cryostat, we estimate the power deposited by γ-radiation to be 2.4 pW to the nuclear stage, 13 pW to the experimental cell, and 7.5 pW

to the stage plate. Despite the disparity in masses of these components, the energy deposited is dominated by the experimental cell and stage plate because of the low transmission factor of the magnet for γ radiation. The corresponding numbers for the power deposited when the cryostat is surrounded by a 5 cm thick lead shield are 0.26, 1.2 and 0.6 pW, consistent with an energy averaged shielding factor of $\sim$10 that is comparable to the reduction in γ counts by a factor of $\sim$20 (see Fig. 2). The difference arises from the preferential shielding of the low energy γ by the lead.

4. ENERGY FLUX FROM COSMIC RAYS

The number used by most low temperature physicists to arrive at an estimate of the heating due to μ cosmic rays is the one quoted by Niinikoski—between 1.5 and 3 cm^{-2} min^{-1}.[10] A more appropriate number is provided in a recent Ref. 22, which gives a value of 1 cm^{-2} min^{-1}, and falls of as $\cos^2\theta$, where θ is the angle between the normal to a horizontal surface and the trajectory of the μ. More complete references are the ones by Rossi,[23,24] and Greisen[21] (see discussion below). Using the same Ge detector that we used to obtain the γ spectra in Fig. 2, we examined the energy range between 2.8 and $\sim$90 MeV, and registered 56158 counts (unshielded) and 48260 counts (with 5 cm shielding) in a 1000 minute interval. The counts were obtained by summing the contents of all the bins of the multichannel analyzer (see Fig. 5). The spectrum shows the range of energies deposited to the Ge detector by individual μ or secondary β particles as they traverse the detector. The spectrum includes a convolution of the size, shape and orientation of the detector, and only weakly reflects (through the Bethe–Bloch equation discussed later) the energy spectrum of the incident particles. Unlike γ quanta, the passage of a μ or β always deposits energy into the detector and no absorption factor correction is necessary.

The total flux of cosmic rays at sea level is[23]

$$I_{v,\mathrm{tot}} = 1.14 \times 10^{-2}\ \mathrm{cm}^{-2}\ \mathrm{s}^{-1}\ \mathrm{sterad}^{-1}, \tag{5}$$

where $I_{v,\mathrm{tot}}$ denotes the total flux of cosmic rays/area-solid angle. The soft component, $I_{v,\mathrm{soft}}$ (generally recognized to be β particles that are emitted following the interaction of a μ as it passes through intervening material such as the concrete slab of the laboratory roof, or the decay of the μ), is obtained by taking the difference between the values obtained in an unshielded and in a heavily shielded (by $\geqslant$10 cm of lead) detector, and is given as[23]

$$I_{v,\mathrm{soft}} = 0.31 \times 10^{-2}\ \mathrm{cm}^{-2}\ \mathrm{s}^{-1}\ \mathrm{sterad}^{-1}. \tag{6}$$

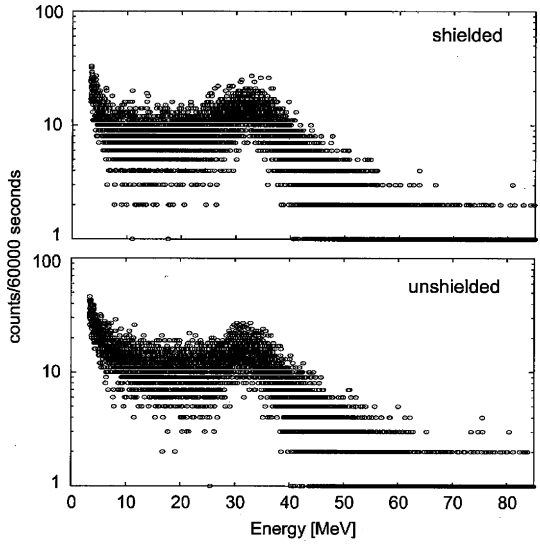

Fig. 5. Counts obtained in a 60000 s time interval for the configuration with 5 cm of lead surrounding the Ge detector (shielded-upper panel) and without the lead (unshielded-lower panel). Each "bin" of the multi-channel analyzer is ~11.5 keV wide. The integrated counts are 56158 and 48260 for the unshielded and 5 cm lead shielded environments. The reduction in counts is due to the "soft" component in the high energy radiation spectrum. As in Fig. 2, the horizontal lines reflect the discrete nature of the counting.

We define the directional flux, $I(\theta)$, where θ is the angle between the normal to a horizontal surface and the direction of the incoming cosmic ray, as $I(\theta) = I_v \cos^2\theta$, where $I(0)$ is the value of I in the vertical direction. Then $I(\theta)d\Omega dS dt$ represents the number of particles incident upon the element of area dS (whose normal is along the θ direction) during the time dt within the element of solid angle $d\Omega$ perpendicular to dS.

The flux J_1 [particles $\mathrm{cm}^{-2}\mathrm{s}^{-1}$] represents the number of particles/second traversing (at all angles) a horizontal element of unit area[24] and can be calculated by carrying out the integration of the directional flux over all angles of incidence. It is given by

$$J_1 = \frac{\pi}{2} I_v. \tag{7}$$

If the unit area is tilted at an angle θ_a to the vertical, J_{θ_a} is given by the expression

$$J_{\theta_a} = \frac{\pi}{2} I_v \left(\cos\theta_a + \frac{\pi}{4}\sin\theta_a\right). \tag{8}$$

The flux through a vertically oriented surface ($\theta_a = \pi/2$), J_3, is given by

$$J_3 = \frac{\pi^2}{8} I_v. \tag{9}$$

Taking the value of $I_{V,\mathrm{tot}}$ from Eq. (5),

$$J_{1,\mathrm{tot}} = \frac{\pi}{2} \times 1.14 \times 10^{-2} \text{ cm}^{-2} \text{ s}^{-1} = 1.79 \times 10^{-2} \text{ cm}^{-2} \text{ s}^{-1},$$
$$J_{3,\mathrm{tot}} = \frac{\pi^2}{8} \times 1.14 \times 10^{-2} \text{ cm}^{-2} \text{ s}^{-1} = 1.41 \times 10^{-2} \text{ cm}^{-2} \text{ s}^{-1}. \tag{10}$$

The geometry of the Ge detector (a cylinder of diameter D=5.33 cm, length L=6.6 cm) oriented with its axis horizontal, provides the means to compare the observed counts to the data from Greisen.[24] The total number of counts observed in this detector in a time t should be $[J_{1,\mathrm{tot}}(DL) + J_{3,\mathrm{tot}}(\pi D^2/4)]t$, where DL is the horizontal "area" of the detector and $\pi D^2/4$ is the vertical area. For $t = 60000$ s, this yields 5.7×10^4 counts, compared to the 56158 counts that we observe in this interval.

If the soft component (see Eq. (6)) were entirely blocked out by the 5 cm thickness of lead, then we should multiply the above by $(I_{v,\mathrm{tot}} - I_{v,\mathrm{soft}})/(I_{v,\mathrm{tot}}) = (1.1.4 - 0.31)/(1.14) = 0.73$. Thus in the case of perfect shielding of the soft component, we should observe $5.67 \times 10^4 \times 0.73 = 4.1 \times 10^4$ counts; we observe 48260. The discrepancy is partially due to the relatively small thickness (5 cm) of the lead used in our experiments. The ratio of shielded to unshielded counts that is observed in our detector is ≈ 0.85

If we apply the same calculation to the silica oscillator (described earlier) which is a vertical rod of diameter $D' = 4.0$ mm and length $L' = 4.2$ cm, the total number of counts observed per second should be $[J_{1,\mathrm{tot}}(\pi D'^2/4) + J_{3,\mathrm{tot}}(D'L')] \times 0.85$, or 2.6×10^{-2} counts/s, compared to our observed value of 2.5×10^{-2} counts/s when the cryostat was shielded with 5 cm lead. [8] In what follows, we use the values of J_1 and J_3 to estimate the heat deposited into the various components of the cryostat.

By carrying out a Monte Carlo calculation for the mean track length for cosmic rays in the germanium detector in which we weighted the tracks with the $\cos^2\theta$ angular dependence of the cosmic ray flux, we find the mean track length to be $\approx 78\%$ of the 5.33 cm diameter of the detector. The total collision loss energy $dE/d(\rho x)$, deposited into the germanium detector can be obtained from the Bethe–Bloch equation[23]

$$\frac{dE}{d(\rho x)} = \frac{2Cm_e c^2}{\beta^2} \left\{ \ln \left\{ \frac{2m_e c^2 E'_m \beta^2}{1-\beta^2} \right\} - 2\beta^2 \right\} \text{MeV cm}^2 \text{ g}^{-1}, \tag{11}$$

where

$$C = \frac{\pi r_0^2 N_A Z}{A}$$

$$E'_m = 2m_e c^2 \frac{p_\mu^2 c^2}{(m_e c^2)^2 + (m_\mu c^2)^2 + 2m_e c^2 m_\mu c^2 \sqrt{p_\mu^2 c^2 + (m_\mu c^2)^2}}$$

$$p_\mu c = \frac{m_\mu c^2 \beta}{\sqrt{1-\beta^2}} = \sqrt{(T_\mu + m_\mu c^2)^2 - (m_\mu c^2)^2}, \ \textit{and} \ \beta = v/c.$$

Here r_0 is the classical radius of the electron (2.82×10^{-13} cm), N_A, is Avogadro's number, Z the atomic number, A the atomic weight and $m_e c^2 = 0.511$ MeV, $m_\mu c^2 = 106$ MeV. T_μ is the kinetic energy of the μ in MeV and v is the speed of one μ. For germanium and a cosmic ray μ having an incoming energy of $\approx$100 MeV, the energy loss is $\approx$ 1.5 MeV cm^2 g^{-1}. This value is smaller than the $\approx$2 MeV cm^2 g^{-1} (see p. 40 and p. 21 in Ref. 16) for a similar track in a-SiO_2 or copper, because of the smaller Z/A for Ge. This yields a peak energy deposited, E_{peak}

$$\begin{aligned} E_{peak} &= (\text{track length}) \times (\text{cross section}) \times (\text{density}) \\ &= (0.78 \times 5.33 \text{ cm}) \times (1.5 \text{ MeV cm}^2 \text{ g}^{-1}) \times (5.36 \text{ g cm}^{-3}) = 33 \text{ MeV}, \end{aligned} \tag{12}$$

close to the 32 MeV peak in Fig. 5. Similarly, we estimate the upper cut-off energy to be 87 MeV (comparable to the upper end of the spectrum in Fig. 5) by accounting for the maximum path length (8.5 cm) and the fact that higher energy μ deposit $\approx$1.8 MeV cm^2 g^{-1}.

In order to calculate the energy deposited by the high energy charged particles into the three massive components that comprise the nuclear stage, we estimate the energy deposited by the passage of a single particle as $\Delta E = 2\text{MeVcm}^2\text{g}^{-1}(\rho.\delta)$, where ρ is the density of the material and δ is the track length (see Eq. (11)). For a cylindrical nuclear stage of length $L = 45$ cm, diameter $D = 4.0$ cm, we estimate $\delta =$ 13 cm using a Monte Carlo numerical simulation technique that takes into account the angular dependence of the particle flux. We then estimate the energy lost per event in the copper nuclear stage as $\Delta E =$ 2 MeV cm^2 g^{-1} $\times$ 8.95 g cm^{-3} $\times$ 13 cm $= 2.3 \times 10^2$ MeV event^{-1} $= 3.7 \times 10^{-11}$ J event^{-1}. Next we calculate the μ flux to the stage $= [J_1(\pi D^2/4) + J_3(DL)] = 2.8$ s^{-1}, which yields a power deposited $\dot{Q}_{stage} = 0.10$ nW. Since the fill factor is $\approx$0.9 and the presence of any slits affects both the average density and the track length, we multiply this heat load by $(0.9)^2$ to

arrive at an estimate of 80 pW. This rate of energy deposition is comparable to the experimentally observed background heat leak of ~100 pW seen in several cryostats which do not have large metallic experimental chambers.[25]

We estimate the power deposited in a 12.5 cm diameter, 1.25 cm thick copper stage plate. Here, $[J_1(\pi D^2/4) + J_3(DL)] = 2.4$ events s^{-1}. The energy deposited / event is given by $\Delta E = 2$ MeV cm^2 $g^{-1} \times 8.95$ g $cm^{-3} \times 1.25$ cm = 23 MeV $event^{-1} = 3.6 \times 10^{-12}$ J $event^{-1}$, and we obtain for the power $\dot{Q}_{\text{stage}} = 3.6 \times 10^{-12}$ J $event^{-1} \times 2.4$ events $s^{-1} = 8.7$ pW. For the 5 cm diameter, 12.5 cm long, experimental cell made from silver, we estimate the mean path to be 7.35 cm. Thus, the energy lost per collision, $\Delta E = 2$ MeV cm^2 $g^{-1} \times 10.5$ g $cm^{-3} \times 7.35$ cm $= 1.5 \times 10^2$ MeV $event^{-1} = 2.5 \times 10^{-11}$J $event^{-1}$. The flux of cosmic rays s^{-1} into the cell is given by $[J_1(\pi D^2/4) + J_3(DL)] = 1.2$ s^{-1}. Thus the power deposited $\dot{Q}_{\text{cell}} = 1.2$ events $s^{-1} \times 2.5 \times 10^{-11}$ J $event^{-1} = 30$ pW. We estimate that this nuclear stage, stage plate and experimental cell experience a heat load of order 120 pW compared to the unshielded heat load due to γ-radition of 21 pW. Once shielded by 5 cm of lead, we expect the reduction of the soft component to reduce the heat load due to cosmic rays to 100 pW, and the γ-radiation to diminish to $\approx$2 pW.

5. THERMAL GRADIENTS

If we add up the heat loads to the experimental cell and the stage plate (in the unshielded case) we arrive at 40 pW due to the cosmic rays and 20 pW due to γ-radiation. If we assume a residual resistance ratio of 1000 for our copper demagnetization stage, then, by using the Wiedemann–Franz law, we arrive at a thermal resistance for the nuclear stage (taking the effective length as 22.5 cm) given by $R_{\text{th}}T = 0.136$ K^2W^{-1}, from which we would predict a minimum temperature that could be attained (ignoring any intervening boundary resistance) of 4 μK. The reduction of the thermal load by attenuating the γ flux and the soft component of the cosmic-rays would reduce the heat load by nearly 50% to 30 pW, resulting in a 25% lower temperature.

It is also instructive to summarize the thermal gradients in the context of two rather different configurations. We consider the effect of the power absorbed in an ultra-low temperature experiment consisting of a silver right circular cylinder of 1 cm diameter and 1 cm length, attached to the cold plate by means of a pressed contact in an unshielded cryostat. The energy deposited by cosmic rays and by γ-radiation would be of order 95 fW and 57 fW, respectively. The pressed contact's electrical resistance is of order 0.1 μΩ,[26] (corresponding to a thermal resistance

given by $R_{\text{th}}T = 4\ \text{K}^2\text{W}^{-1}$) and the limiting temperature in the experiment would be of order 1 μK (we ignore the thermal resistance of the intervening copper demagnetization stage discussed above). The number of ineractions/sec due to cosmic rays is expected to be 0.028 s^{-1}, compared to the 0.08 $\text{s}^{-1}\gamma$ quanta that would interact with the silver (2% of the flux). In contrast, a sample of silica glass of similar size would experience a smaller heat load (because of its lower density) of order 30 fW, but because of the large thermal boundary resistance (of order 13 $T^{-3}\ \text{K}^4\ \text{W}^{-1}$,[7]), the silica sample would be limited to ~1 mK irrespective of the temperature of the nuclear stage. In addition, as illustrated in Fig. 1, radiation may have an effect beyond the heat deposition calculated here.

6. CONCLUSION

We performed acoustic measurements in amorphous silica Suprasil-W using a torsional oscillator that revealed the presence of low level background radiation and the influence of cosmic rays on insulating disordered solids. This motivated us to estimate the heat deposited to ultra-low temperature cryostats by these radiation sources. We outlined the procedure to calculate the heat load due to both cosmic ray μ and local low-level background γ-radiation to a model nuclear stage (that is shielded from γ-radiation quite effectively by the large superconducting magnet) and experiments that are not shielded from γ-radiation by the magnet. The heating due to γ-radiation was calculated to be 20 pW compared to the 120 pW heating due to cosmic rays. We showed that enclosing the cryostat in a 5 cm thick lead wall reduced the overall heating to the nuclear stage by ~30% from 140 to 100 pW. These residual heat inputs are close to those measured on other similar shape nuclear refrigerators, and suggests that most of the residual heat leaks are due to low level radiation.

In our experiment on amorphous SiO_2, the introduction of lead shielding reduced the number of interactions with γ and cosmic rays by approximately a factor of three. The power deposited (by γ and cosmic ray radiation) to a 1 cm diameter × 1 cm long amorphous glass sample was calculated to be 30 fW, but the large boundary resistance results in a limiting temperature of order 1 mK irrespective of the cryostat temperature. A smaller sample aspect ratio (length area^{-1}) should improve matters somewhat.

To conclude, essentially all of the γ flux and part of the cosmic ray derived flux can be shielded out using a 5 cm thick layer of lead shielding around the cryostat which may prove to be critical in many experiments.

ACKNOWLEDGMENTS

Support was provided by the NSF under DMR-0202113, 0071630 and INT-0128811 and by the Cornell Center for Materials Research under DMR-0079992. We acknowledge early contributions of R.M. Merithew and helpful discussions with Y. Bunkov. Finally, we thank the personnel at Wilson Laboratory at Cornell for lending us the lead bricks.

REFERENCES

1. K. Gloos, P. Smeibidl, C. Kennedy, A. Singsaas, P. Sekowski, R. M. Mueller, and F. Pobell, *J. Low Temp. Phys.* **73**, 101 (1988).
2. D. J. Cousins, S. N. Fisher, A. M. Guenault, R. P. Haley, I. E. Miller, G. R Pickett, G. N. Plenderleith, P. Skyba, P. Y. A. Thibault, and M. G. Ward, *J. Low Temp. Phys.* **114**, 547 (1999).
3. M. V. Hobden and N. Kurti, *Phil. Mag.* **4**, 1092 (1959).
4. K. Andres and O. V. Lounasmaa, in *Progress in Low Temp. Phys.* D. F. Brewer, ed., North Holland, Amsterdam (1982), Vol.VIII p. 221.
5. M. Schwark, M. Kubota, R. M. Mueller, and F. Pobell, *J. Low Temp. Phys.* **58**, 171 (1985).
6. D. G. Cahill and J. E. van Cleve, *Rev. Sci. Instr.* **60**, 2706 (1989).
7. E. Thompson, G. Lawes, J. M. Parpia, and R. O. Pohl, *Phys. Rev. Lett.* **84**, 4601 (2000).
8. E. Nazaretski, R. D. Merithew, R. O. Pohl, and J. M. Parpia, *J. Low Temp. Phys.* **134**, 407 (2004).
9. E. Nazaretski, R. D. Merithew, V. O. Kostroun, A. T. Zehnder, R. O. Pohl, and J. M. Parpia, *Phys. Rev. Lett.* **92**, 245502-1 (2004).
10. T. Niinikoski, *Liquid and Solid Helium, Proc. of the European Phys. Soc., Haifa 1974,* C. G. Kuper, S. G. Lipson, and M. Revzen Eds., Wiley, New York (1975), p. 145.
11. A. J. Leggett, *Phys. Rev. Lett.* **53**, 1096 (1984).
12. P. Schiffer and D. D. Osheroff, *Rev. Mod. Phys.* **67**, 491 (1995) and references therein. Y. M. Bunkov and O. D. Timofeevskaya, *Phys. Rev. Lett.* **80**, 4927 (1998).
13. M. Niemetz and W. Schoepe, *J. Low Temp. Phys.* **135**, 447 (2004).
14. E. Nazaretski, S. Dimov, R. O. Pohl, and J. M. Parpia, accepted for publication in *J. Low Temp. Phys.,* 2004.
15. E. Nazaretski, R. D. Merithew, J. M. Parpia, and R. O. Pohl, submitted to *Phys. Rev. B.,* 2004.
16. A. W. Wolfendale, *Cosmic Rays*, George Newnes, London (1963).
17. http://physics.nist.gov/physRefData/Xcom. Also E. Storm and H. I. Israel, *Nucl. Data Tables, A* **7**, 565 (1970).
18. H. Becker, M. S. Thesis, MPI Kernphysik, Heidelberg, 1991 (unpublished).
19. M. J. Martin and P. H. Blichert-Toft, *Nuclear Data Tables* **A8**, 1 (1970)
20. T. Shutt, B. Ellman, P. D. Barnes, Jr., A. Cummings, A. Da Silva, J. Emes, Y. Giraud Héraud, E. E. Haller, A. E. Lange, R. R. Ross, J. Rich, B. Sadoulet, G. Smith, W. Stockwell, C. Stubbs, N. Wang, S. White, B. A. Young, and D. Yvon, *Phys, Rev. Lett.* **69**, 3425 (1992).
21. M. Deguchi, I. Tomisawa, T. Oka, N. Abe, and K. Kawano, *Adv. in ESR Appl.* **18**, 289 (2002).
22. K. Hagiwara *et al., Phys. Rev. D* **66**, 010001 (2002).
23. B. Rossi, *Rev. Mod. Phys.* **20**, 537 (1948).
24. K. Greisen, *Phys. Rev.* **61**, 212 (1942).
25. F. Pobell, *Physica B* **109–110**, 1485 (1982).
26. M. Manninen and W. Zimmermann Jr., *Rev. Sci. Instr.* **48**, 1710 (1977).